JOURNAL OF SOLID STATE CHEMISTRY 118, 193–198 (1995)

BRIEF COMMUNICATION

Lithium Insertion Characteristics of $CuNb_2O_6$

M. Sato[1] and Y. Hama

Department of Chemistry and Chemical Engineering, Faculty of Engineering, Niigata University, Niigata 950-21, Japan

Received April 20, 1994; in revised form January 27, 1995; accepted January 27, 1995

Chemical and electrochemical lithium intercalation reactions of $CuNb_2O_6$ with a columbite structure were examined. The chemical lithiation by *n*-butyllithium occurred accompanied by the formation of a new phase, $Li_xCuNb_2O_6$ ($0 \leqq x \leqq 1.9$), with an apparent crystal lattice. The *a* axis of the new phase is a little longer (0.6 Å) than that of the parent phase. The electrochemical cell potential of $Li/CuNb_2O_6$ almost attained a plateau at 2.6 V against Li/Li^+ in the range from $x = 0.1$ to $x = 1.0$ in $Li_xCuNb_2O_6$, corresponding to the reduction from Cu^{2+} to Cu^+. The reduction behavior in the range from $x = 1.0$ to $x = 1.9$ suggested the reduction from Nb^{5+} to Nb^{4+}.

INTRODUCTION

The lithium intercalation reaction has been investigated on various transition metal oxides by chemical or electrochemical methods because it is an important reaction in cathode materials in secondary lithium batteries (1). These oxides can be characterized as affording an open structure for the accommodation of lithium ions and by involving metal ions with high valence states, *i.e.*, $LiMn_2O_4$ (2–4) and LiV_2O_4 (3), with a spinel-type structure, or $LiCoO_2$ (5, 6) and $LiNiO_2$ (7, 8), with an α-$NeFeO_2$ structure. All these compounds have a cubic close-packed (ccp) oxygen array, which offers cavities or tunnels in which to incorporate lithium ions.

In addition to these oxides, some oxides containing divalent copper ions, *e.g.*, CuV_2O_6 (9, 10) and $CuV_{2-x}Mo_xO_6$ (11), have recently received attention as cathode materials because they exhibit good electrode properties in terms of both energy density and cycle performance, although the cell voltage of the cathodes prepared by them is somewhat lower, ranging from 2.5 to 3.0 V *vs.* Li/Li^+. In these oxides, the lithium insertion occurs comparatively easily, accompanied by a small expansion of the interlayer spacing. Cu^{2+} ions participate in the redox reaction to form Cu^+ ions and sometimes metallic Cu in the deep lithiation levels (12). Similar lithium intercalation reactions associated with Cu^{2+} ions are reported on CuO (13), $LiCuVO_4$ (14), and $CuTa_2O_6$ (15).

We recently reported on the synthesis and crystal structure of $LiCuM_3O_9$ (M = Ta, Nb) compounds (16), which have essentially the same crystal structure as that of $CuTa_2O_6$, with a defect perovskite structure (17). These oxides show a lithium intercalation reaction by using *n*-butyllithium (18). Although the crystal structures of both $LiCuNb_3O_9$ and $LiCuTa_3O_9$ are the same as that of $CuTa_2O_6$, $CuNb_2O_6$ does not crystallize in any perovskite structure, but rather, in a columbite structure (19). In the columbite structure, the main framework of the crystal lattice is built up of hexagonal close-packed (hcp) oxygen arrays, in contrast to the $CuTa_2O_6$ defect perovskite, where ccp oxygen arrays exist. Some of the octahedral sites formed by the fcp arrays are vacant. These facts enable us to investigate the lithium intercalation reaction on $CuNb_2O_6$. In this study, the lithium intercalation is done both chemically and electrochemically, and the possible sites for inserted lithium ions in the crystal lattice is discussed on the basis of the structure.

EXPERIMENTAL

$CuNb_2O_6$ was prepared by a solid state reaction of reagent grade CuO and Nb_2O_5 powders. The appropriate quantities of the reactants were ground together in an agate mortar and the mixture was pressed (40 MPa) into pellets. They were heated at 900–1200°C in an alumina crucible for 12 hr in air. The products obtained were analyzed by a powder X-ray diffractometer (Rigaku, Geiger flex 2035) and confirmed to be single-phase $CuNb_2O_6$ referring to JCPDS data (No. 39-1493).

The structural refinement of the sample was obtained by Rietveld analysis. A powder X-ray diffraction pattern for the refinement was obtained with a high power X-ray diffractometer (Rigaku, RAD-rA) equipped with a curved-crystal graphite monochrometer using $CuK\alpha$ radiation. The data were collected on thoroughly ground powders by the step-scanning method in the 2θ range from 10° to 110° with a step width of 0.02° and a scan time of 4 sec. The powder pattern obtained was analyzed using the RIETAN profile refinement program (20).

[1] To whom correspondence should be addressed.

0022-4596/95 $12.00

TABLE 1
Positional Parameters and Anisotropic Thermal Parameters for $CuNb_2O_6$ Refined on the Basis of *Pbcn*

		Atomic parameters[a]			
Atom	Site	x	y	z	B (Å)
Cu	4c	0.0	0.3305(9) (0.3304)	0.25	—
Nb	8*d*	0.1592(1) (0.1596)	0.1829(3) (0.1824)	0.7822(2) (0.7814)	—
O(1)	8*d*	0.0931(6) (0.0916)	0.1025(17) (0.1006)	0.0925(19) (0.1000)	0.3(3)
O(2)	8*d*	0.4159(5) (0.4158)	0.1009(16) (0.0956)	0.1531(19) (0.1472)	0.2(1)
O(3)	8*d*	0.7594(8) (0.7583)	0.1292(18) (0.1267)	0.0485(19) (0.0444)	0.2(1)

Anisotropic thermal parameters[b]

Atom	β_{11}	β_{22}	β_{33}	β_{12}	β_{13}	β_{23}
Cu	0.0004(2)	0.0020(19)	0.0135(25)	0.0	0.0005(6)	0.0
Nb	0.0005(1)	0.0032(6)	0.0046(7)	0.0001(4)	0.0001(3)	0.0006(7)

Note. The cell parameters are a = 14.1038(2) Å, b = 5.60728(8) Å, and c = 5.12375(8) Å. R Factors (defined in Ref. (20)) are R_{wp} = 4.70%, R_p = 3.44%, R_E = 4.47%, R_I = 2.52%, and R_F = 2.36%.

[a] The atomic coordinates in parentheses are those reported by Ref. (22).

[b] The form of anisotropic thermal parameters is $\exp[-(h^2\beta_{11} + k^2\beta_{22} + l^2\beta_{33} + 2hk\beta_{12} + 2hl\beta_{13} + 2kl\beta_{23})$. β_{12} and β_{23} are fixed at zero for Cu atom in the 4c site.

For chemical lithiation into $CuNb_2O_6$, *n*-butyllithium (*n*-BuLi) in *n*-hexane solution was added as reducing agent for $CuNb_2O_6$ powder dispersed in *n*-hexane at 25°C under an argon atmosphere. The concentrations of *n*-BuLi were varied from 0.17 to 1.60 mole dm^{-3}, to control the extent of the lithium insertion into the sample. The amount of the inserted lithium was denoted by x in $Li_xCuNb_2O_6$, which was determined by a flame spectrochemical analyzer (Hitachi, 180-50), using an aqueous LiCl solution as a standard.

Composite electrodes for the electrochemical lithiation were made by mixing the active material of $CuNb_2O_6$, with acetylene black (Denki Chemical, Denka black) used as a conductor and polytetrafluoroethylene (Daikin, Polyflon D-1) used as a binder, in a weight ratio of 8 : 1 : 1. The mixture was compression-molded on a Ni net under about 10 MPa. The pellet thus obtained was used as a positive electrode after being dried at 280°C for 20 min, the geometric surface area of which was about 2.10 cm^2. Lithium plates cut from lithium metal ingots were used for both the negative and the reference electrodes. Each of three electrodes was separated with polypropylene membrane sheets soaked with the electrolyte in the electrochemical cell. The electrolyte was made of 1 mole dm^{-3} $LiClO_4$ dissolved in a 1 : 1 mixture of propylene carbonate (PC) and dimethoxyethane (DME), containing only trace amounts of water, less than 100 mg dm^{-3}. The electrochemical lithium insertion was done galvanostatically with a potentiostat/galvanostat (Hokuto Denko, HA501). The cyclic voltammetric analysis was carried out in the potential range 1.5–4.0 V against the lithium reference electrode with a scanning rate of 0.5 mV min^{-1}. The potentiostat/galvanostat and a function generator (Hokuto Denko, HB-104) were used for this measurement. The cells were assembled in a glove box filled with argon.

RESULTS AND DISCUSSION

It is known that there are two polymorphs reported for $CuNb_2O_6$, in accordance with the preparation temperatures (21). One is a black orthorhombic phase prepared at relatively high temperatures (>1100°C), and the other a yellowish-green monoclinic phase prepared at low temperatures. Although the two phases are different in color, they have essentially the same cell dimensions. Recently,

TABLE 2
Bond Distances (Å)[a] for $CuNb_2O_6$ Refined on the Basis of *Pbcn*

CuO_6 polyhedron	
Cu–O(1)	2.002(9) × 2 (1.976)
Cu–O(2)$^{(1)}$	1.987(9) × 2 (1.973)
Cu–O(2)$^{(2)}$	2.412(9) × 2 (2.383)
NbO_6 polyhedron	
Nb–O(1)$^{(3)}$	1.897(9) (1.941)
Nb–O(1)$^{(4)}$	2.092(10) (2.073)
Nb–O(2)$^{(1)}$	1.741(9) (1.773)
Nb–O(3)$^{(5)}$	2.068(10) (2.047)
Nb–O(3)$^{(6)}$	2.265(11) (2.267)
Nb–O(3)$^{(7)}$	1.963(11) (1.964)
Average	2.003

Note. Symmetry code: none x, y, z; (1) $-1/2 + x$, $1/2 + y$, $1/2 - z$; (2) x, $1 - y$, $1/2 + z$; (3) x, y, $1 + z$; (4) x, $-y$, $1/2 + z$; (5) $1 - x$, y, $1/2 - z$; (6) $1 - x$, $-y$, $1 - z$; (7) $-1/2 + x$, $1/2 - y$, $1 - z$.

[a] The distances in parentheses are those reported by Ref. (22).

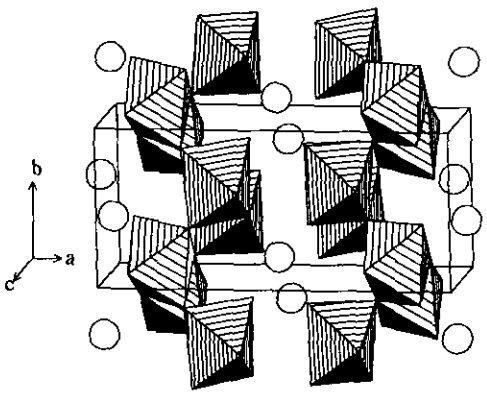

FIG. 1. Orthorhombic crystal structure refined for yellowish-green phase of $CuNb_2O_6$. The projection is along the nearly c direction. NbO_6 octahedra and copper atoms are shown as shaded polyhedra and open circles, respectively.

Drew *et al.* (22) prepared a single crystal of the black phase and determined the crystal structure. In this work, we have obtained several samples prepared at various temperatures. The samples prepared below 900°C were always a mixture of the yellowish-green phase and the starting materials, while the samples prepared at temperatures over 1100°C consisted of the black phase. In the case of the preparation temperatures ranging from 900 to 1100°C, the color of the samples changed from yellowish-green to black with increasing preparation temperature, indicating a mixture of the black and yellowish-green phases. The SEM analysis clearly showed that the sample prepared at 900°C consists of microcrystalline particles (about 1 μm) with homogeneous size distribution, while the sample prepared at 1100°C consists of larger crystalline particles (about 15 μm). Since the fine crystalline particles are considered to be very favorable as cathode materials in lithium batteries, we used the sample prepared at 900°C for further investigation.

All the reflections of the powder X-ray diffraction pattern for the sample were indexed on the basis of monoclinic symmetry. The most probable space group was found to be $P2_1/c$ with cell parameters of a = 5.507(1) Å, b = 14.103(1) Å, c = 5.123(1) Å, and β = 90.0(1)°, which are very close to those reported by Drew *et al.* (22). Interestingly, all the reflections were also completely indexed on the orthorhombic *Pbcn* space group, which corresponds to the space group of the black phase. The cell parameters for *Pbcn* are essentially the same as those for $P2_1/c$. For both space groups, the Rietveld structural refinement was performed. The coordinates for all the atoms reported for the black phase (22) were adopted as an initial structural model. The least-squares refinement led to R_{wp} = 4.60% for $P2_1/c$ and R_{wp} = 4.70% for *Pbcn*. In the case of $P2_1/c$, the isotropic thermal parameters refined for all the oxygen atoms, however, converged to negative values, and some of the metal–oxygen bond distances were quite short. On the other hand, the crystallographic parameters refined for *Pbcn* all converted to normal values. The positional and thermal parameters refined for *Pbcn* are listed in Table 1 and the interatomic distances and angles are listed in Table 2. Apparently, our data are very close to those reported for the black phase (22). At present, it is unknown which space group is true for the yellowish-green phase of $CuNb_2O_6$. The atomic coordinates refined for $P2_1/c$ were found to be quite compatible with those for *Pbcn*. Therefore, this fact, at least, indicates that the fundamental framework of the columbite structure is realized in the yellowish-green phase.

Figure 1 shows the projection along the nearly [010] direction of the structure refined for orthorhombic *Pbcn*. A polyhedron of oxygen atoms forming hcp arrays is the main structural feature. Each NbO_6 octahedron shares two edges with adjoining NbO_6 octahedra which form zigzag chains running along the c direction. Two of these chains associate at their corners to form double chains. The discussion concerning the crystal structure in this study is based on the crystallographic data refined for *Pbcn*.

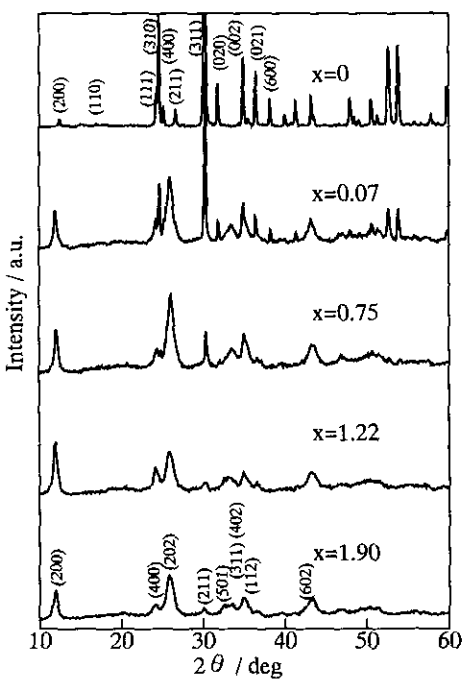

FIG. 2. Powder X-ray diffraction patterns of lithium intercalated products, $Li_xCuNb_2O_6$, prepared with n-butyllithium at various concentrations. Indices for the sample with x = 0 are based on the *Pbcn* space group and those for the sample with x = 1.90 are based on the *Pcan* space group.

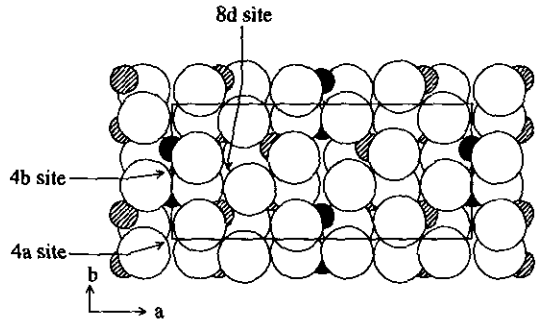

FIG. 3. Stacking sequence of atoms in $CuNb_2O_6$ projected along the c direction. Oxygen, niobium, and copper atoms are shown as large open circles, shaded circles, and filled circles, respectively.

In the reduction processes of copper and niobium components upon the lithium insertion of $CuNb_2O_6$, the structural changes were investigated by powder X-ray diffraction measurements for the products intercalated step by step with various concentrations of *n*-BuLi. Typical X-ray diffraction patterns are given in Fig. 2. Similar behavior in the chemical intercalation was also observed for the black phase prepared at 1100°C. The rate of the intercalation reaction for this phase was much less than the yellowish-green phase. This could be due to the larger crystalline particles of the black phase. The maximum amount of the chemical lithium intercalation was found to be about 1.90 molecules per unit formula. Surprisingly, only a small amount of lithium insertion into $CuNb_2O_6$ brings about a new phase. With increasing values of x, the new phase becomes more abundant in the intercalated product. Since the peak of the (311) reflection belonging to the columbite structure disappears up to the lithium intercalation level of $x = 1.22$, the columbite structure seems to transform completely to the new phase when being inserted by about one mole of lithium ions, probably corresponding to the reduction from Cu^{2+} to Cu^{+}. It can be seen in the X-ray diffraction pattern that the new phase still retains an apparent crystal lattice although its crystallinity becomes poorer. The indexing of the reflection peaks of the new phase was attempted. A solution with a fairly high reliability was obtained when an orthorhombic crystal system was assumed, whose cell parameters are nearly $a = 14.7$ Å, $b = 3.60$ Å, and $c = 7.75$ Å, with possible space groups of *Pcna* (standard expression, *Pban*) and *C*222. Although the structural refinement for the new phase was not successful because of its fairly poor crystallinity, some structural information can be drawn from the lattice parameters. The lattice parameters estimated for the new phase are intimately correlated with those of the parent $CuNb_2O_2$, *i.e.*, $a_n \fallingdotseq a$, and $b_n \fallingdotseq (b + c)/\sqrt{2}$, $c_n \fallingdotseq \sqrt{2}(b + c)$, where the subscript n's correspond to the lattice parameters of the new phase. The length of the a axis, which expresses the stacking sequence unit of the hcp oxygen atom arrays shown in Fig. 3, becomes a little longer (about 0.6 Å) accompanied by the lithium intercalation. In the columbite structure, there are three kinds of empty octahedral sites, *i.e.*, $4a(0, 0, 0)$, $4b(0, 1/2, 0)$, and $8d(x, y, z)$ with $x \fallingdotseq 1/6$, $y \fallingdotseq 1/2$, and $z \fallingdotseq 0$ as indicated in Fig. 3. Among these octahedral sites, the lithium ions inserted into $8d$ sites would seem to have a large repulsive interaction subject to adjacent Nb^{5+} ions. The environment for $4a$ and $4b$ sites is inherently almost identical in a "normal" columbite structure, such as $CaNb_2O_6$. But, in the structure of $CuNb_2O_6$, the $4b$ sites are compressed due to the Jahn–Teller deformation of adjacent CuO_6 octahedra, as shown in Fig. 4, while the $4a$ sites are relatively open. Such deformation of the $4b$ sites would become relaxed if the Jahn–Teller Cu^{2+} ions disappear. Therefore, it is reasonable that lithium insertion occurs at the $4a$ sites in the first stage, and then at the $4b$ sites in the following stage. On the assumption that both $4a$ and $4b$ sites can accommodate lithium ions with full occupancy, the formula of the intercalated product corresponds to $x = 2$ in $Li_xCuNb_2O_6$, which is almost consistent with the results of the chemical lithium intercalation. Since no diffraction peaks for metallic copper are seen in the reaction products (Fig. 2), possible reduction processes are thought to be $Cu^{2+} \rightarrow Cu^{+}$ for all copper ions in the first stage and $Nb^{5+} \rightarrow Nb^{4+}$ for half of the niobium ions in the next stage. The existence of two such reduction species is also pointed out for the lithium intercalation reaction of the defect perovskite $LiCuNb_3O_9$ (18). The reduction process of $Cu^{2+} \rightarrow Cu^{+}$ can give a lattice relaxation due to the disappearance of Jahn–Teller Cu^{2+} ions, leading to a fairly small expansion (0.6 Å) of the a axis. The three kinds of empty octahedra in a columbite structure are isolated

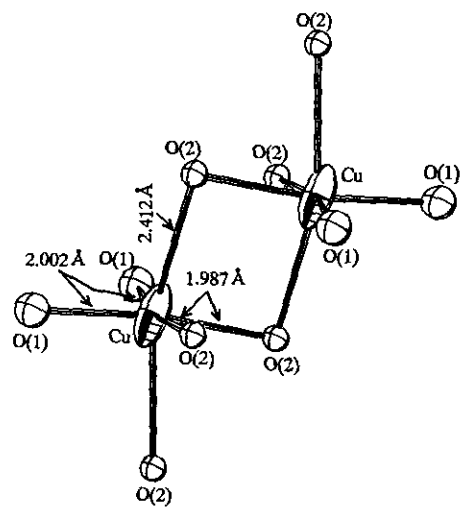

FIG. 4. Environment around two adjacent copper atoms.

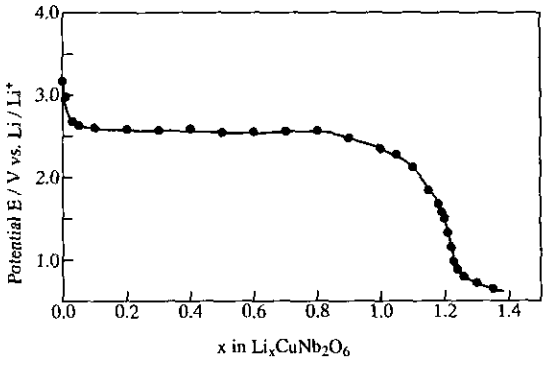

FIG. 5. Discharge curve of a $Li/CuNb_2O_6$ cell at a current density of 0.1 mA cm^{-2}.

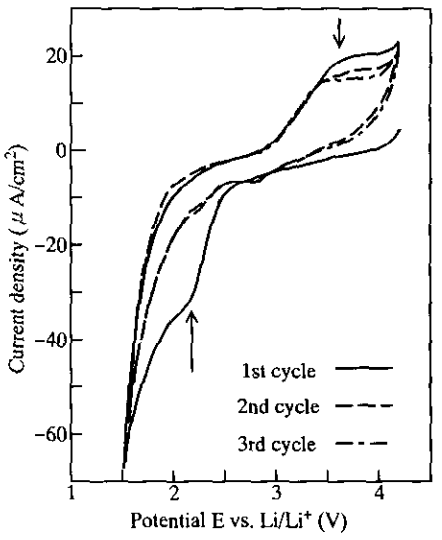

FIG. 6. Cyclic voltammogram of a $Li/CuNb_2O_6$ cell at a potential scanning rate of 0.5 mV min^{-1}.

from each other. This is the crucial difference from spinel-type $LiMn_2O_4$, in which empty tetrahedral and octahedral sites are interconnected through face-sharing with each other (3). Therefore, an intercalation reaction in $CuNb_2O_6$ is thought to proceed accompanied by the formation of intercalated phase domains, not the formation of continuous solid solutions.

Figure 5 shows the electrode potentials of electrochemical lithium insertion under a relatively low current density of 0.1 mA cm^{-2}. Except for the first potential drop, the electrode potential vs x curve in the range from 0 to 1.0 becomes more or less flat. The cell voltage in the plateau region is about 2.6 V, quite comparable to that of Li $CuVO_4$ (14). Apparently, this region corresponds to a coexistence state of the intercalated new phase and the parent phase, as indicated by X-ray diffraction patterns for the chemical intercalation (Fig. 2). Furthermore, this region is also consistent with the first reduction stage being $Cu^{2+} \rightarrow Cu^{+}$, and the region, after a steep drop of the electrode potential at around $x = 1.0$, is probably due to the next reduction stage of $Nb^{5+} \rightarrow Nb^{4+}$.

Figure 6 shows the cyclic voltammogram in the potential range from 1.5 to 4.0 V at a scanning rate of 0.5 mV min^{-1}. In the reduction process of the first cycle, a slight shoulder is observed at about 2.2 V. This reduction current disappeared for the following cycles. As the potential for this reduction current is compatible with that of the plateau region in Fig. 5, this reduction reaction may correspond to the reduction of $Cu^{2+} \rightarrow Cu^{+}$ and is irreversible. Large reduction currents can be seen below this potential, due to the reduction of $Nb^{5+} \rightarrow Nb^{4+}$. The oxidation currents at 3.5 V in every cycle seem to responsible for this reduction reaction. Therefore, the redox reaction concerning niobium ions is reversible. The irreversibility of the redox reaction concerning copper ions is thought to be attributed to the high energy necessary for the Jahn–Teller distortion.

ACKNOWLEDGMENTS

We are indebted to Mr. K. Uematsu for his help in the flame spectrochemical analysis of the samples. Funding for a portion of this work by the Iketani Science and Technology Foundation is also gratefully acknowledged.

REFERENCES

1. J. Desilverstro and O. Haas, *J. Electrochem. Soc.* **137,** 5C (1990).
2. W. I. F. David, M. M. Thacheray, L. A. De Picciotto, and J. B. Goodenough, *J. Solid State Chem.* **67,** 316 (1986).
3. B. Zachau-Christiansen, K. West, T. Jacobsen, and S. Atlung, *Solid State Ionics* **40/41,** 580 (1990).
4. M. M. Thacheray, A. De Koch, M. H. Rossouw, D. Liles, R. Bittihn, and D. Hoge, *J. Electrochem. Soc.* **139,** 363 (1992).
5. T. Nagaura and K. Tozawa, *Prog. Batteries Sol. Cells* **9,** 209 (1990).
6. J. N. Reimers and J. R. Dahn, *J. Electrochem. Soc.* **139,** 2091 (1992).
7. J. R. Dahn, U. Von Sacken, and C. A. Michel, *Solid State Ionics* **44,** 87 (1990).
8. M. Antaya, J. R. Dahn, J. S. Preston, E. Rossen, and J. N. Reimers, *J. Electrochem. Soc.* **140,** 575 (1993).
9. Y. Sakurai, H. Ohtsuka, and J. Yamaki, *J. Electrochem. Soc.* **135,** 32 (1988).
10. Y. Sakurai, S. Tobishima, and J. Yamaki, *Electrochim. Acta* **34,** 981 (1989).
11. Y. Takeda, K. Itoh, R. Kanno, T. Ichikawa, N. Imanishi, and O. Yamamoto, *J. Electrochem. Soc.* **138,** 2566 (1991).
12. A. Tranchant, R. Messina, and J. Perichon, *J. Electroanal. Chem.* **242,** 181 (1988).
13. S. J. Hibble, C. Malitesta, and P. G. Dickens, *Solid State Ionics* **39,** 289 (1990).
14. R. Kanno, Y. Kawamoto, Y. Takeda, M. Hasegawa, and O. Yamamoto, *Solid State Ionics* **40/41,** 576 (1990).
15. N. Kumada, S. Hosoda, F. Muto, and N. Kinomura, *Inorg. Chem.* **28,** 3592 (1989).
16. M. Sato and Y. Hama, *J. Mater. Chem.* **3,** 233 (1993).

17. H. Vincent, B. Bochu, J. J. Aubert, J. C. Joubert, and M. J. Marezio, *J. Solid State Chem.* **24,** 245 (1978).
18. M. Sato, T. Jin, Y. Hama, and K. Uematsu, *Bull Chem. Soc. Jpn.* **66,** 2255 (1993).
19. J. Felton, *J. Inorg. Nucl. Chem.* **29,** 1168 (1967).
20. F. Izumi, *Nippon Kesshou Gakkaishi* **27,** 23 (1978).
21. E. Wahlström and B-O. Marinder, *Inorg. Nucl. Chem. Lett.* **13,** 559 (1977).
22. M. G. B. Drew, R. J. Hobson, and V. T. Padayatchy, *J. Mater. Chem.* **3,** 889 (1993).